

Particle decay in the early universe: predictions for 21 cm

Yu. A. Shchekinov^{1*} and E. O. Vasiliev^{2,3†}

¹*Department of Physics, University of Rostov, Sorge St. 5, Rostov-on-Don, 344090 Russia*

²*Tartu Observatory, 61602 Tõravere, Estonia*

³*Institute of Physics, University of Rostov, Stachki Ave. 194, Rostov-on-Don, 344090 Russia*

Accepted 2006 December 15. Received 2006 April 1; in original form 2006 April 1

ABSTRACT

The influence of ultra-high energy cosmic rays (UHECRs) and decaying dark matter particles on the emission and absorption characteristics of neutral hydrogen in 21 cm at redshifts $z = 10 - 50$ is considered. In presence of UHECRs 21 cm can be seen in absorption with the brightness temperature $T_b = -(5 - 10)$ mK in the range $z = 10 - 30$. Decaying particles can stimulate a 21 cm signal in emission with $T_b \sim 50 - 60$ mK at $z = 50$, and $T_b \simeq 10$ mK at $z \sim 20$. Characteristics of the fluctuations of the brightness temperature, in particular, its power spectrum are also calculated. The maps of the power spectrum of the brightness temperature on the plane *wavenumber-redshift* are shown to be sensitive to the parameters of UHECRs and decaying dark matter. Observational possibilities to detect manifestations of UHECRs and/or decaying particles in 21 cm with the future radio telescopes (LOFAR, 21CMA and SKA), and to distinguish contributions from them are briefly discussed.

Key words: early Universe – cosmology:theory – dark matter – diffuse radiation.

1 INTRODUCTION

At $z \sim 1000$ the Universe enters the “dark ages” epoch, the electrons and protons recombine, and gas remains neutral until the first luminous objects emerge at $z \sim 30 - 20$. Neutral gas can be observed in a redshifted 21 cm line of neutral hydrogen in emission or absorption against the cosmic microwave background (CMB). This gives a possibility for studying the processes associated with transition of the neutral universe into a fully ionized state, and for identification of the sources responsible for reionization (Hogan & Rees 1979, Madau et al 1997). At present observations of 21 cm line are anticipated as a promising tool for diagnostics of the universe in the end of “dark ages” (Madau et al 1997, Tozzi et al 2000, Ciardi & Madau 2003).

Possible sources of photons which can be important for reionization form two different groups. The first, connected with conventional baryon physics, involves the baryons processed in stellar nucleosynthesis (Shapiro & Giroux 1987, Miralda-Escudé & Rees 1994, Tegmark et al 1994, Cen 2003, Ciardi et al 2003, Choudhury & Ferrara 2006) and in shock waves near black holes (Madau et al 1999, Oh 2001, Ricotti & Ostriker 2004). The other is connected with unstable dark matter and can include massive neutrinos (Sciama 1982, Scott et al 1991), superheavy X-particles (Berezinsky et al 1997, Kuzmin & Rubakov, 1998, Birkel & Sarkar,

1998). The first luminous objects are commonly thought to be the principal source of the reionization. They heat gas in the universe through ionization by ultraviolet (UV) and X-ray photons. This inevitably affects the emissivity of gas in the 21 cm line, because the hydrogen spin temperature T_s depends on the gas kinetic temperature T_k , and thus observed intensity imprints the effects from the objects of the first generation (Madau et al 1997, Tozzi et al 2000, Ciardi & Madau 2003, Loeb & Zaldarriaga 2004, Zaldarriaga et al 2004, Chen & Miralda-Escudé 2004, Sethi 2005).

Production of copious number of ionizing photons during the dark ages can be connected also with the origin of ultra-high energy cosmic ray (UHECRs) if they form from decaying superheavy dark matter (SHDM) particles with masses $M_X \gtrsim 10^{12}$ GeV in the so-called top-to-bottom scenario (Berezinsky et al 1997, Kuzmin & Rubakov, 1998, Birkel & Sarkar, 1998). The associated production of UV photons can have strong influence on cosmological recombination (Doroshkevich & Naselsky 2002, Doroshkevich et al 2003).

Decaying dark matter particles, such as massive neutrinos, can also contribute significantly to reionization (Sciama 1982, Dodelson & Jubas 1994). Initial polarisation measurements of the CMB by the Wilkinson Microwave Anisotropy Probe (WMAP) satellite (Spergel et al 2003) imparted a new impulse to this possibility. The obtained relatively large optical depth of the universe $\tau \simeq 0.16$ suggested unrealistically strong constraints on properties of the first stellar objects (e.g. Cen 2003, Wyithe & Loeb 2003, see also an

* E-mail: yus@phys.rsu.ru

† E-mail: eugstar@mail.ru

alternative discussion in Tumlinson et al 2004), which lead some to consider that decaying dark matter can be at least a complementary source of reionization (Hansen & Haiman 2004, Chen & Kamionkowski 2004 (hereafter CK), Kasuya et al 2004, Kasuya & Kawasaki 2004, Pierpaoli 2004, Mapelli et al 2006). The corresponding heating can change characteristics of 21 cm in emission and absorption. Very recently, the influence of dark matter decay and annihilation on the 21 cm line from dark ages has been also considered by Furlanetto et al. (2006a) for long living particles. For the models with similar parameters of decaying particles they reached conclusions close to ours.

In this paper we study the effects of UHECRs and decaying particles on cosmological 21 cm background. We assume a Λ CDM cosmology with the parameters $(\Omega_0, \Omega_\Lambda, \Omega_m, \Omega_b, h) = (1.0, 0.76, 0.24, 0.041, 0.73)$ (Spergel et al 2006).

2 SPIN TEMPERATURE

The two processes: atomic collisions and scattering of UV photons, couple the HI spin temperature and the gas kinetic temperature (Wouthuysen 1952, Field 1958)

$$T_s = \frac{T_{cmb} + y_a T_k + y_c T_k}{1 + y_a + y_c} \quad (1)$$

here T_{cmb} is the CMB temperature, y_c, y_a are the functions determined by the collisional excitations and the intensity of the UV resonant photons

$$y_a = \frac{P_{10} T_*}{A_{10} T_k}, \quad y_c = \frac{C_{10} T_*}{A_{10} T_k} \quad (2)$$

$T_* = 0.0682$ K is the hyperfine energy splitting, $A_{10} = 2.87 \times 10^{-15} \text{ s}^{-1}$ is the spontaneous emission rate of the hyperfine transition, $C_{10} = k_{10} n_H + \gamma_e n_e$ is the collisional de-excitation rate by hydrogen atoms and electrons, the rate by protons is negligible, for k_{10} we use the approximation by Kuhlen et al (2006), for γ_e we take the approximation from Liszt (2001), P_{10} is the indirect de-excitation rate, which is related to the total Ly α scattering rate P_a (Field 1958)

$$P_{10} = 4P_a/27, \quad (3)$$

where

$$P_a = \int c n_\nu \sigma_\nu d\nu, \quad (4)$$

n_ν is the number density of photons per unit frequency range, $\sigma(\nu)$ is the cross section for Ly α scattering (Madau et al 1997). The brightness temperature in 21 cm is then (Field 1958, Chen & Miralda-Escudé 2004)

$$T_b = 25\text{mK} \frac{T_s - T_{cmb}}{T_s} \left(\frac{\Omega_b h_0}{0.03} \right) \left(\frac{0.3}{\Omega_{m0}} \right)^{1/2} \left(\frac{1+z}{10} \right)^{1/2}. \quad (5)$$

It is worth mentioning here that recently Hirata & Sigurdson (2007) showed that the spin temperature depends in general on atomic velocities $T_s = T_s(v)$, if excitation and de-excitation collisional processes are dominated by interatomic (H-H and H-He) collisions. This effect results in a sufficiently strong (up to 60%) increase of the 21-cm line width, however only in a 2% decrease of the emissivity. In this paper we focus mostly on the total emissivity, and therefore neglect these effects. In principle, such a widening of the

21 cm line can be important in the power spectrum of the brightness temperature on very small scales, $\lambda \lesssim 3$ kpc.

3 IONIZATION AND THERMAL HISTORY OF THE UNIVERSE

Evolution of the fractional ionization is described by

$$\frac{dx_e}{dz} = \frac{1}{(1+z)H(z)} (R_s(z) - I_s(z) - I_e(z)) \quad (6)$$

where besides the standard recombination and ionization rates $R_s(z), I_s(z)$, the term $I_e(z)$ is explicitly introduced due to presence of additional sources of UV photons. For the UHECRs this term can be written in the form (Peebles et al 2000, Doroshkevich & Naselsky 2002)

$$I_e(z) = \epsilon(z) H(z) x_H, \quad (7)$$

where $\epsilon(z) = \epsilon_0/(1+z)$ is the production of ionizing photons, $H(z)$ is the Hubble parameter, x_H is the fraction of neutral hydrogen. For decaying particles this term is written as (CK)

$$I_e(z) = \chi_i f_x \Gamma_X \frac{m_p c^2}{h\nu_c} \quad (8)$$

where χ_i is the energy fraction deposited into ionization for which we made use the calculations by Shull & van Steenberg (1985), m_p is the proton mass, $f_x = \Omega_X(z)/\Omega_b(z)$, $\Omega_b(z)$ is the baryon density parameter, $\Omega_X(z)$ is the fractional abundance of decaying particles, Γ_X is the decay rate, $h\nu_c$ is the energy of Ly-c photons. For short living particles $\Omega_X(z) \propto e^{-\Gamma_X t}$ and their contribution to ionization and heating essentially vanishes at $t > \Gamma_X^{-1}$; normally Γ_X^{-1} is assumed to be comparable to the comoving Hubble time in the range of redshifts of interest.

The gas temperature is determined by equation

$$(1+z) \frac{dT}{dz} = 2T + k_C \frac{x_e}{H(z)(1+f_{He}+x_e)} (T - T_{cmb}) - \frac{2}{3k} \frac{K}{H(z)(1+f_{He}+x_e)} \quad (9)$$

where the second term in the r.h.s. describes the energy exchange between the gas and CMB photons $k_C = 4.91 \times 10^{-22} T_{CMB}^4$, $f_{He} = 0.24$, the third term is the heating from additional sources of the ionizing photons, K is the corresponding heating rate which can be written in the form (CK)

$$K = \chi_h m_p c^2 f_x \Gamma_X \quad (10)$$

where χ_h is the energy fraction depositing into heating; as for χ_i we used for χ_h the results of Shull & van Steenberg (1985). By order of magnitude $\chi_i \sim \chi_h \sim 1/3$ for the conditions we are interested in.

In the presence of UHECRs the final products are only Ly α and Ly-c photons (Doroshkevich & Naselsky 2002). As pointed out by (Chen & Miralda-Escudé 2004) the injected Ly α photons change the gas temperature very little: $K_\alpha = 0$. Ly-c photons have the energy slightly in excess of the hydrogen binding energy: $\sim 13.6 \text{ eV} + 3kT/2$. Therefore the heating rate from the UHECRs produced Ly-c photons K_c has to be calculated self-consistently together with equation (10). However, as we will see later the gas kinetic

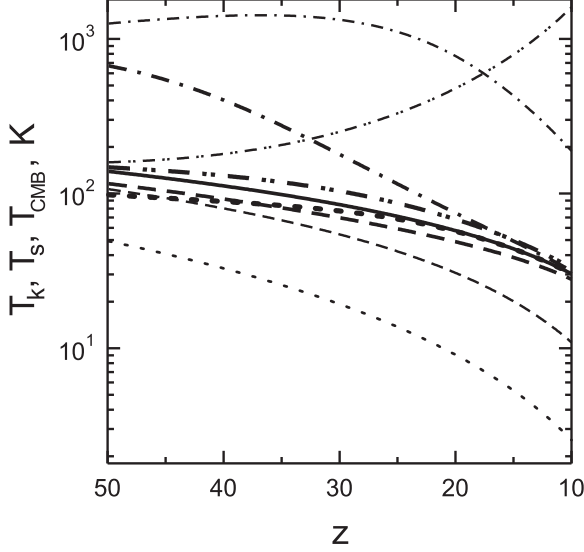


Figure 1. The kinetic (thin lines), spin (thick lines) and CMB (thick solid line) temperatures for the standard recombination $\epsilon = 0$ (dashed), in the presence of UHECRs for the UV production rate $\epsilon = 1$ (dotted), and in the presence of decaying particles: long living with $\xi = 3 \times 10^{-26} \text{ s}^{-1}$ (dot-dot dashed), and short living with $\Gamma_X = 10^{-15} \text{ s}^{-1}$, $f_X(z_{eq}) = 10^{-8}$ (dash-dotted).

temperature in presence of UHECRs is at most 150 K, so that the heating rate from Ly-c photons is always less than $\sim 2 \times 10^{-31} \epsilon (1+z)^{3/2} \text{ erg cm}^{-3} \text{ s}^{-1}$. The corresponding contribution to the gas kinetic temperature is less than a few percent.

We apply a modified version of the code RECFAST (Seager et al 1999) to solve equations (6), (10).

4 RESULTS

Stellar and quasi-stellar sources of ionizing radiation begin to form at redshifts $z < 20$, and gas around them heated through photoionization can emit in 21 cm with a spot-like distribution. The spots have too small angular sizes, and can be detected only later, when at $z \lesssim 15$ star formation increases and forms pervading domains of sufficiently hot gas (Zaroubi & Silk 2004). Instead, UV photons from additional ionizing sources, like UHECRs and decaying particles, illuminate and heat the IGM homogeneously, and therefore the signal from 21 cm can be more easily detected from the earliest redshifts.

Fig. 1 shows kinetic and spin temperatures for a selected set of ionizing photon production rates by UHECRs and decaying particles. For the standard history ($\epsilon = 0$) the spin temperature is nearly equal to the CMB value at $z \leq 20$, and the intergalactic gas cannot produce distinguishable signal in 21 cm in this redshift range. The kinetic temperature for UHECRs with $\epsilon = 1$ is more than twice of the value in the standard ionization history ($\epsilon = 0$). The increase of kinetic temperature for higher ϵ is due to an increase of the

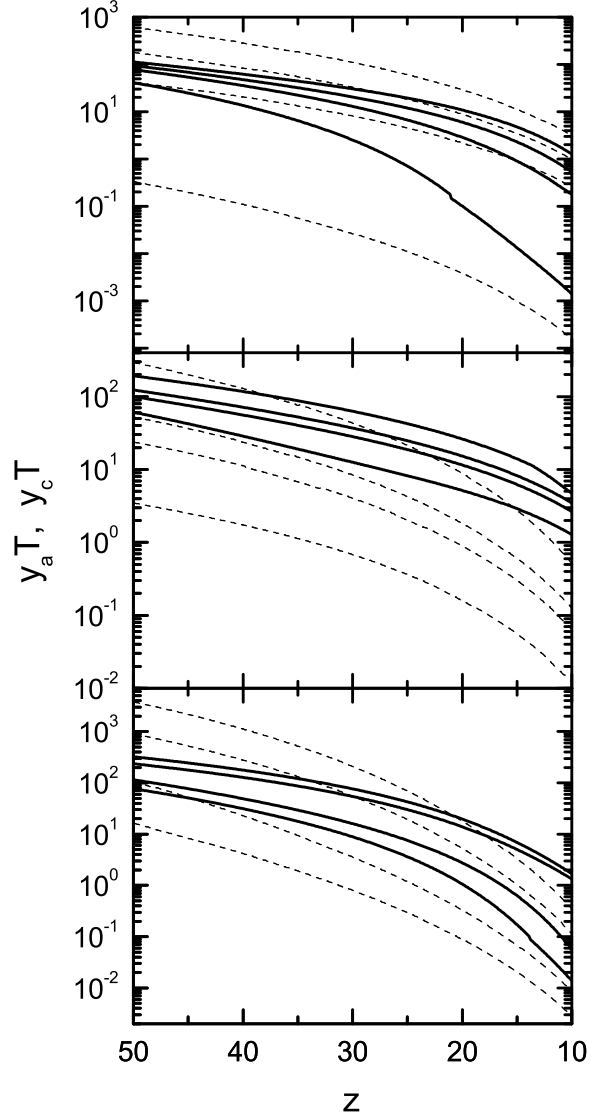


Figure 2. The contributions to the spin temperature from collisions (thick solid lines) and photon excitations (thin dashed lines) for the models with UHECRs *upper panel* for $\epsilon = 0, 0.3, 1, 3$ from bottom to top; long living particles *mid panel*: $\xi = 6 \times 10^{-27} \text{ s}^{-1}$, $3 \times 10^{-26} \text{ s}^{-1}$, $6 \times 10^{-26} \text{ s}^{-1}$, $3 \times 10^{-25} \text{ s}^{-1}$ – from the lowermost to the uppermost; $\xi = \chi_i f_X \Gamma_X$, and short living *lower panel* decaying particles: $\Gamma_X = 10^{-14} \text{ s}^{-1}$, $f_X(z_{eq}) = 0.5 \times 10^{-8}$, $\Gamma_X = 5 \times 10^{-15} \text{ s}^{-1}$, $f_X(z_{eq}) = 10^{-8}$, $\Gamma_X = 10^{-15} \text{ s}^{-1}$, $f_X(z_{eq}) = 10^{-8}$, $\Gamma_X = 10^{-15} \text{ s}^{-1}$, $f_X(z_{eq}) = 5 \times 10^{-8}$ – from the lowermost to the uppermost.

fractional ionization of gas and a stronger coupling between the CMB photons and electrons. As a result, the gas kinetic temperature in this case shows similar variation with z as the CMB temperature. Due to collisional de-excitations of the hyperfine structure level this increase in T_k unavoidably results in a decrease of the spin temperature, such that the difference between the spin and CMB temperature in the range $z \sim 35 - 10$ is for $\epsilon = 1$ greater than for $\epsilon = 0$;

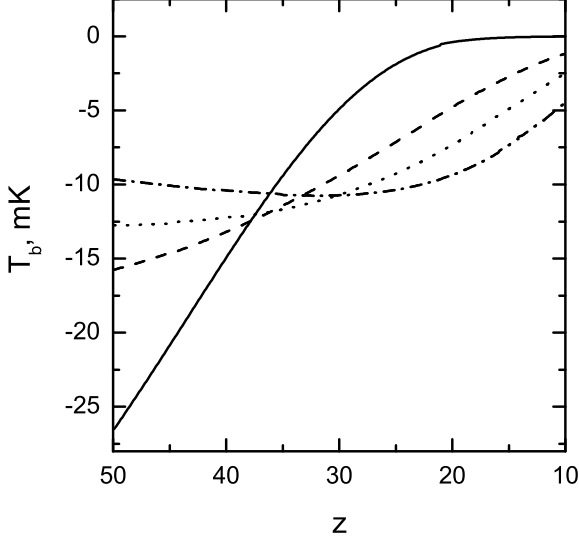


Figure 3. The brightness temperature in the presence of UHECRs for the UV production rate $\epsilon = 0$ (solid), $\epsilon = 0.3$ (dashed), $\epsilon = 1$ (dotted), $\epsilon = 3$ (dash-dotted).

$T_s - T_{CMB}$ vanishes at $z \leq 10$. This means that the signal in 21 cm can be detected in the redshift range $z \sim 10 - 35$ in absorption. The long living particles provide a permanent heating the injection energy rate $3k\dot{T}/2 = K/(1 + f_{He} + x_e)$, such that for a sufficiently high heating (ionization) rate shown in Fig. 1 the gas kinetic temperature in this case grows towards lower z as seen in Fig. 1 (thin dot-dot dashed line). Contrary, the short living particles inject heat with the rate $\dot{T} \propto e^{-\Gamma x^t}$, which manifests in a relatively fast decrease of the kinetic temperature at low z (thin dash-dotted line in Fig. 1). The HI spin temperature remains in both cases above the CMB temperature.

As mentioned above, the heating of gas in models with UHECRs is small, and therefore the deviation of the brightness temperature from the standard value is mostly due to the Wouthuysen-Field (WF) effect from the UV photons produced by UHECRs. In Fig. 2 we show the contributions of heating (collisional excitation and de-excitation) and Wouthuysen-Field effect to the spin temperature for UHECRs and decaying particles.

Fig. 3 presents brightness temperature versus redshift for several values of ϵ . An obvious qualitative difference between the standard model ($\epsilon = 0$) and the models with $\epsilon \geq 0.3$ is clearly seen: contrary to the standard case in all models T_b flattens at $z > 30$ at the level $T_b \simeq -(10 - 15)$ mK. On the other hand at $z < 25$, where the standard model shows almost zero T_b all models with $\epsilon \geq 0.3$ have brightness temperature between -5 and -10 mK. The signal of tens mK can though be easily swamped by a much stronger (of $\gtrsim 100$ K) foreground emission at meter wavelengths. However, multi-frequency observations seem to allow one to remove the foreground, which is expected to be featureless in frequency space (Shaver et al. 1999, Di Matteo et al. 2002, Oh & Mack 2003, Gnedin & Shaver 2004, Zaldarraga et

al. 2004). One can hope thus that an 1000 hours LOFAR (Low Frequency Array) and/or SKA (Square Kilometre Array) observation can discriminate between the standard and $\epsilon \geq 0.3$ models (see discussion in Sect. 4).

Spatial variations of the brightness temperature connected with density perturbations in emitting gas are to be more easily distinguished in the redshifted 21 cm emission. For this purpose we calculated the derivative of the brightness temperature T_b over the amplitude of the density fluctuation δ , where the perturbed density field is assumed in the form $\rho = \rho_0(z)(1 + \delta)$, with $\rho_0(z)$ being the background baryon density. We calculated the deviations of the spin and kinetic temperatures starting from $z_0 = 1000$ and followed the evolution of perturbed regions according to equation (10) to the redshift of interest z , accounting the dependence of kinetic coefficients k_{10} and γ_e on temperature. In Fig. 4 we show results for the standard recombination model: the upper panel of Fig. 4a illustrates the deviation δT_b of the local brightness temperature from the all-sky one for a separate perturbation of a given density amplitude δ . As expected, the overdense regions show larger amplitude in absorption. The dependence of δT_b on redshift (x -axis) weakens at higher z . For the sake of clarity in the lower panel of Fig. 4a we show also the derivative $dT_b/d\delta$ versus redshift and amplitude: at $z = 20 - 40$ it weakly depends on the amplitude δ , although changes very sharp versus redshift. The total signal comprises contributions from the whole spectrum of perturbations and is represented by the temperature power spectrum (Barkana & Loeb 2005ab, Hirata & Sigurdson 2007)

$$P_{T_b} = P_{\mu^0}(k) + \mu^2 P_{\mu^2}(k) + \mu^4 P_{\mu^4}(k), \quad (11)$$

where $\mu = k_{||}/k$ is the cosine of the angle between the line of sight and the wavevector,

$$\begin{aligned} P_{\mu^0} &= \left(\frac{\partial T_b}{\partial \delta} \right)^2 P_\delta(k), \\ P_{\mu^2} &= k \bar{T}_b \frac{\partial T_b}{\partial \delta} P_{\delta,v}(k), \\ P_{\mu^4} &= k^2 \bar{T}_b^2 P_v(k), \end{aligned} \quad (12)$$

\bar{T}_b is the mean brightness temperature, $P_\delta(k)$, $P_v(k)$ are the power spectrum of the baryon density and velocity fluctuations, $P_{\delta,v}(k)$, their cross-spectrum. Fig. 4b shows $\delta T_b(k, z) = \sqrt{k^3 P_{T_b}/2\pi^2}$ for the standard model in the plane (z, k) : the dominant contribution stems from the density fluctuations, the contribution from density-velocity cross-spectrum is always around 20-30 %, the velocity fluctuations contribute less than 10-20 % at $z \leq 40$, and increases (up to 30%) at $z \sim 50$; these estimates are given for the average (over 4π) value of $\mu^2 = 1/3$.

In Fig. 5 we show the distributions δT_b , $dT_b/d\delta$ and $\delta T_b(k, z)$ for the model with UHECRs $\epsilon = 1$. As in the standard model 21 cm line can be observed in absorption, however there is a clearly seen distinct feature between the two cases: the standard model shows gradient of the temperature power spectrum from low amplitudes and redshifts (right bottom corner in Fig. 4b) towards higher amplitudes and redshifts (left upper corner), while the model with UHECRs reveals an opposite behaviour of the gradient of $\delta T_b(k, z)$ – from the left lower to the right upper corner, and in addition, a much smaller gradient in redshift (i.e. in frequencies) at lower amplitudes.

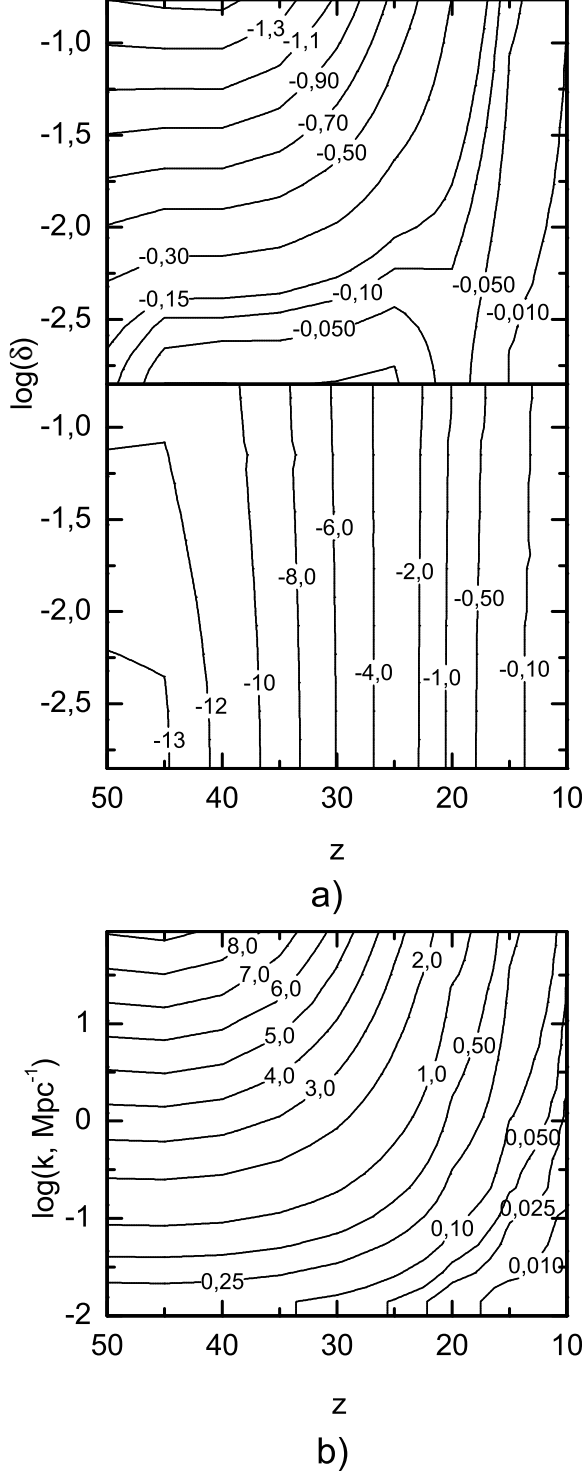


Figure 4. a) The difference between the local and all-sky brightness temperatures $\delta T_b = T_b(\delta) - T_b$ (upper panel), the derivative $dT_b/d\delta$ (lower panel) as functions of redshift and density variation δ ; b) the temperature power spectrum $\delta T_b(k, z)$ as a function of redshift and wavenumber k : standard model. Numbers on isocontours are given in mK.

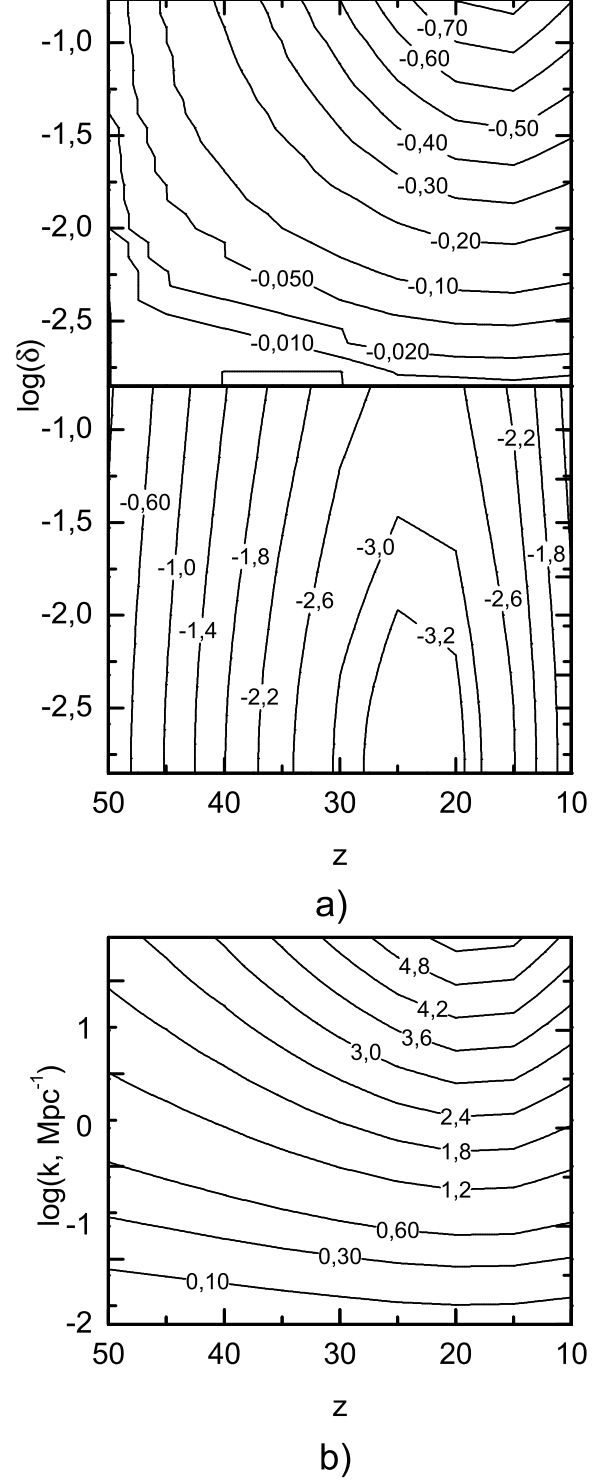


Figure 5. Same as in Fig. 4 for model with UHECRs: $\epsilon = 1$.

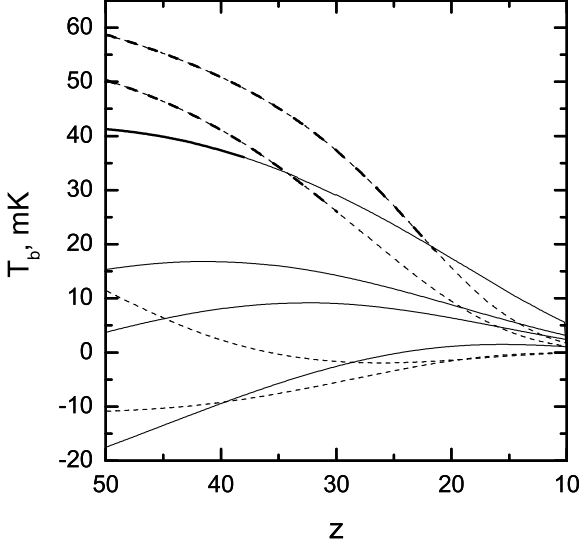


Figure 6. *Solid lines* – the brightness temperature in the presence of long living particles $\Gamma_X \ll H_0$: $\xi = 6 \times 10^{-27} \text{ s}^{-1}$, $3 \times 10^{-26} \text{ s}^{-1}$, $6 \times 10^{-26} \text{ s}^{-1}$, $3 \times 10^{-25} \text{ s}^{-1}$ – from the lowermost to the uppermost; $\xi = \chi_i f_X \Gamma_X$. *Dashed lines* – the brightness temperature in the presence of short living particles $\Gamma_X \gtrsim H_0$: $\Gamma_X = 10^{-14} \text{ s}^{-1}$, $f_X(z_{eq}) = 0.5 \times 10^{-8}$, $\Gamma_X = 5 \times 10^{-15} \text{ s}^{-1}$, $f_X(z_{eq}) = 10^{-8}$, $\Gamma_X = 10^{-15} \text{ s}^{-1}$, $f_X(z_{eq}) = 10^{-15} \text{ s}^{-1}$, $f_X(z_{eq}) = 10^{-8}$, $\Gamma_X = 10^{-15} \text{ s}^{-1}$, $f_X(z_{eq}) = 5 \times 10^{-8}$ – from the lowermost to the uppermost; the thick part of the solid curve and the dot-dashed thick parts of the dashed curves indicate the predominance of WF effect.

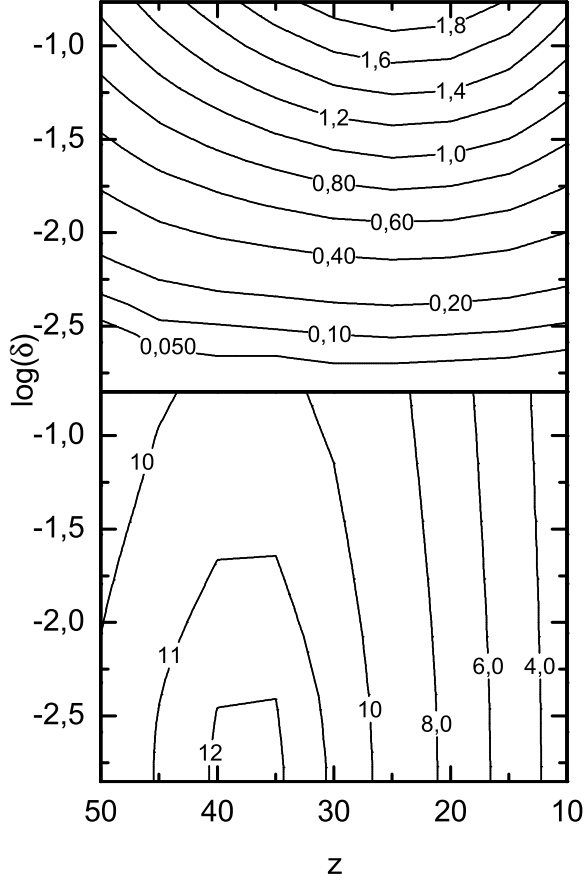
The models with decaying dark matter can produce 21 cm in emission and in absorption as well. Fig. 6 shows the all-sky brightness temperature for the long living (solid lines) and short living (dashed lines) decaying particles. The gas kinetic temperature grows with heating rate and can be lower or greater than T_{cmb} depending on ξ . Therefore, at low heating rate ($\xi \leq 6 \times 10^{-27} \text{ s}^{-1}$) gas can be observed in 21 cm only in absorption with a lower absolute brightness temperature than in the standard case, essentially approaching it due to decrease in the heating rate (compare the lower solid line in Fig. 6 with the solid line in Fig. 3). The transition from absorption to emission occurs at $\xi \geq 10^{-26} \text{ s}^{-1}$. The long living decaying particles affect the spin and the brightness temperature mostly through collisional heating (as seen in Fig. 2), however in some cases Wouthuysen-Field effect can become more important: this is the model with $\zeta = 3 \times 10^{-25} \text{ s}^{-1}$ at $z > 40$ – the contribution from WF effect is shown in Fig. 6 as a thick part of the corresponding curve.

Brightness temperature for short living particles T_b increases with the heating rate similar to what occurs for the long living particles, and correspondingly at a sufficiently high heating 21 cm can be observed in emission. There is, however, a qualitative difference between the dependence of brightness temperature on redshift in these two cases: for the long living particles $T_b(z)$ has always negative sec-

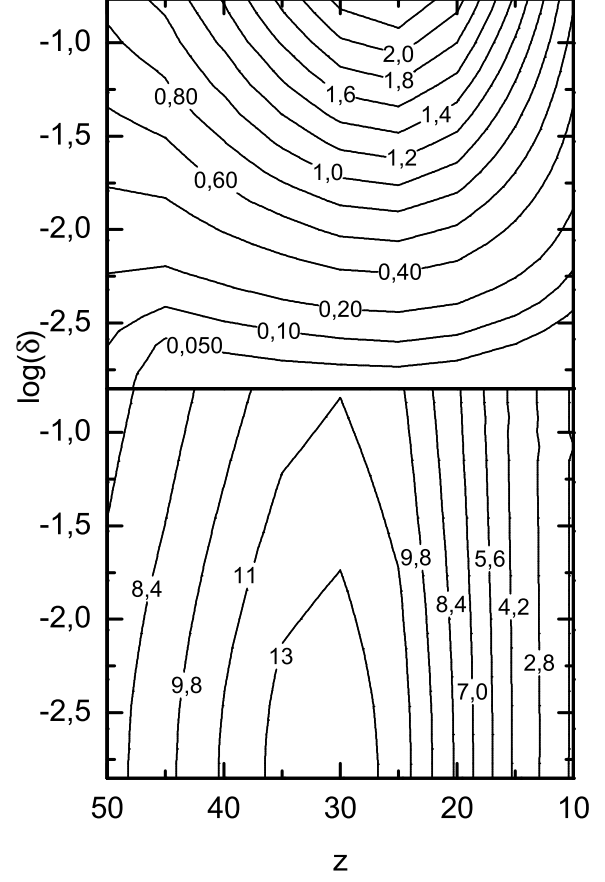
ond derivative, while in the case of the short living particles $T_b(z)$ has an inflection point. Note in this connection that $T_b(z)$ curves in models with the UHECRs have always positive second derivative. Similarly to the models with long living decaying particles, for short living particles a mostly collisional (heating) contribution to T_s and T_b is reversed to predominantly Wouthuysen-Field effect for the models with $\Gamma_X = 10^{-15} \text{ s}^{-1}$ and $f_X(z_{eq}) = 10^{-8}$, and with $\Gamma_X = 10^{-15} \text{ s}^{-1}$, $f_X(z_{eq}) = 5 \times 10^{-8}$ at $z > 30$ and $z > 20$, respectively; this is also shown by the thick parts of the corresponding curves in Fig. 6. The inflection point on $T_b(z)$ nearly corresponds to redshifts where WF effect becomes dominating.

The differences between the second derivatives of the all-sky brightness temperature $T_b(z)$ is reflected to a certain extent on the behaviour of the temperature power spectra on (z, k) plane. As seen in Fig. 7b the lines of equal spectral power for the long living particles reveal a smooth, nearly uniform, gradient over the whole range of redshifts and wavenumbers (amplitudes). At the same time, for the short living particles (Fig. 8b) these lines thicken at the low z side, with a stronger gradient, similarly to the model with UHECRs where $d^2 T_b / dz^2$ is always positive. The behaviour of the temperature difference δT_b and its derivative $dT_b/d\delta$ on the (z, k) plane are also distinct for these two models of decaying particles (Fig. 7a and 8a): the short living particles show thickening near the low end of redshifts. These differences though are not well pronounced (as, for instance, between the standard model and the model with UHECRs shown in Fig. 4 and 5), and it seems to be challenging to reveal them. In the high redshift end $z > 20$ (lower frequencies), the $\delta T_b(k, z)$ maps for the two models look quite similar. However, at $z < 20$ (higher frequencies) the temperature power spectrum at a given wavenumber decreases towards lower redshift faster in the model with short living particles, which can be recognizable in the frequency space.

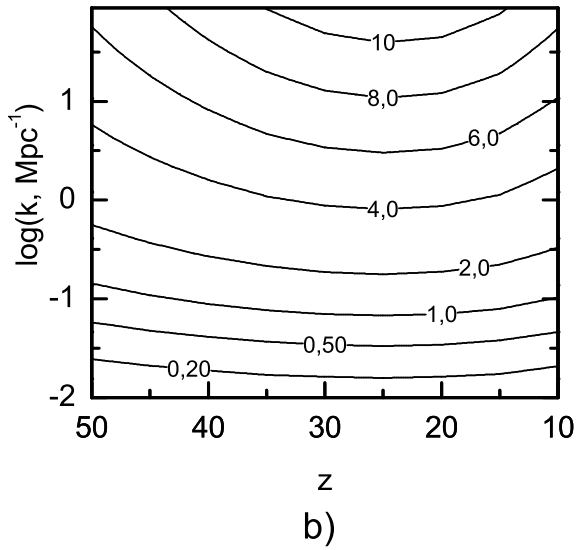
The differences between the second derivatives of the all-sky brightness temperature over redshift $d^2 T_b / dz^2$ for the models with UHECRs and long- and short living particles, or the corresponding differences between the temperature power spectra, imprint in spectral features of the 21 cm line. This circumstance may have a principal significance for choosing a strategy for observational discrimination between manifestations from the three sources of the ionizing photons, provided that observations are possible for a wide range of redshifts, from $z = 10$ to $z = 50$. However, if the qualitative difference between $T_b(z)$ and $\delta T_b(k, z)$ curves for the UHECRs and long living particles seems to be relatively easily observationally distinguishable, it looks problematic for the curves $T_b(z)$ and $\delta T_b(k, z)$ in cases with the long and short living particles because the inflection of $T_b(z)$ in the latter case lies within $\Delta T_b(z) \simeq 5 \text{ mK}$, and the differences between the $\delta T_b(k, z)$ maps are basically within a few mK for wavenumbers from, e.g., 0.1 to 1 Mpc^{-1} . From this point of view “two-color” diagrams, connecting the differences between the brightness temperatures at different wavelengths, can be complementary to the analysis of $T_b(z)$ curves and $\delta T_b(k, z)$ maps. We show an example of such “two-color” diagrams for the three sources of UV photons: UHECRs, long and short living decaying particles in Fig. 9. Specifically, we plot the relative all-sky temperature differences $\Delta^2 T_{23} = \Delta T_b(\lambda_2) - \Delta T_b(\lambda_3)$ versus $\Delta^2 T_{12} = \Delta T_b(\lambda_1) - \Delta T_b(\lambda_2)$, where $\lambda_1 = 210 \text{ cm}$, $\lambda_2 = 420$



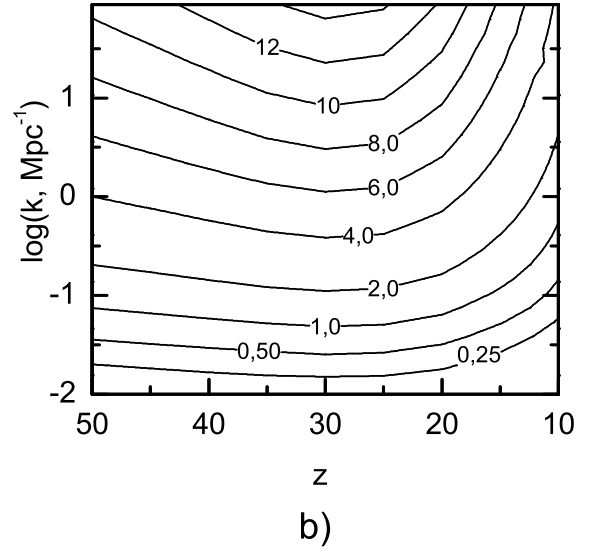
a)



a)



b)



b)

Figure 7. Same as in Fig. 4 for the model with long living particles $\Gamma_X \ll H_0$ for $\xi = 6 \times 10^{-26} \text{ s}^{-1}$.

Figure 8. Same as in Fig. 4 for the model with short living particles $\Gamma_X \gtrsim H_0$: $\Gamma_X = 10^{-15} \text{ s}^{-1}$, $f_X(z_{eq}) = 10^{-8}$.

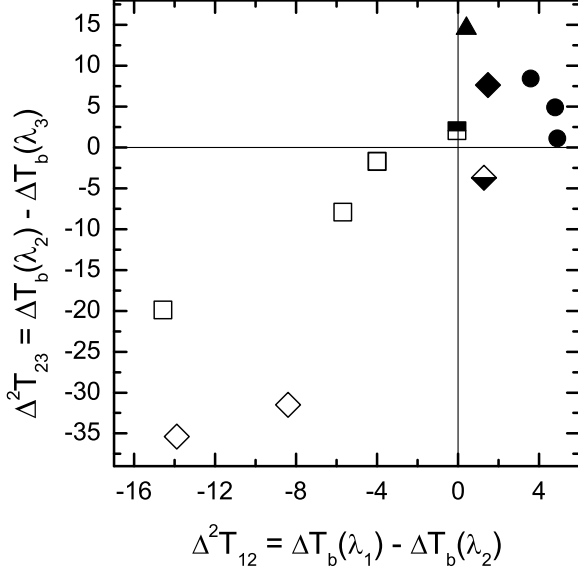


Figure 9. “Two-color” diagram for the models with UHECRs and decaying particles. Open symbols show differences in brightness temperatures in emission, filled – in absorption; half-filled correspond to emission at low z (lower half is open) and absorption at high z (upper half is filled), and vice versa. Circles show ($\Delta^2 T_{12}, \Delta^2 T_{23}$) for UHECRs, diamonds – for long living decaying particles, squares – for short living particles, the triangle depicts the standard (no additional ionizing photons) case.

cm, $\lambda_3 = 840$ cm, for a set of models for these three cases, here $\Delta T_b(\lambda_i)$ is the difference between the total signal at $\lambda_i = 21(1 + z_i)$ cm and the temperature of the foreground emission at this wavelength. Since the foreground emission has temperature of several orders of magnitude higher than the expected from 21 cm, determination of the 21 cm signal with using such a subtraction procedure seems challenging. However, as pointed out by Di Matteo et al. (2002), and Oh & Mack (2003), the perspectives for measurements of the all-sky signal from redshifted 21 cm are not totally dim because the foreground emission is expected to be featureless in frequency (see also discussion in Zaldarriaga et al. 2004, Sethi 2005). The three cases fall into quite distinct regions in the “two-color” plane with a separation of $\Delta^2 T > 5$ mK, and thus can in principle be discriminated observationally.

The parameters of decaying particles and UHECRs we explored in this work are consistent with the current constraints. CK found using WMAP data $\xi < 10^{-24} \text{ s}^{-1}$ for the long living particles, and a slightly weaker upper limit for the short living ones. Recent results from WMAP give a lower value of the optical depth $\tau \lesssim 0.09$ (Spergel et al 2006). This strengthens the constraints on the parameters of decaying particles compared to those inferred from the WMAP data of the first year. However, as pointed out by CK decaying particles with short lifetimes do not affect significantly the optical depth and are thus less constrained. On the other hand, the upper limit for $\xi = 3 \times 10^{-25} \text{ s}^{-1}$ for long living particles, we consider here, lies within the re-

strictions on possible ionization rates corresponding to the optical depth obtained from the third year WMAP data. For UHECRs Doroshkevich & Naselsky (2002) inferred from the MAXIMA-1 and BOOMERANG data (de Bernardis et al 2000, Hanany et al 2000) $\epsilon \leq 3$. Observations of HI at $z = 10 - 50$ in 21 cm can provide further constraints.

The sensitivity of ongoing long-wavelength experiments, such as LOFAR, 21CMA (former PAST), MWA, LWA, SKA and LUDAR (Carilli 2006) seems to be sufficient to detect signal in 21 cm affected by decaying particles and UHECRs at pre-ionization epochs. The minimum background source flux density required to detect an absorption feature with the signal to noise ratio S/N is (Furlanetto 2006)

$$S_{min} = 16 \left(\frac{S/N}{5} \right) \left(\frac{10^{-3}}{\tau} \right) \left(\frac{10^6 \text{ m}^2}{A_{eff}} \right) \times \left(\frac{T_{sys}}{400 \text{ K}} \right) \left(\frac{100 \text{ kHz}}{\Delta\nu} \frac{1 \text{ week}}{t_i} \right)^{0.5} \text{ mJy} \quad (13)$$

where τ is the optical depth in 21 cm, A_{eff} is the effective area of telescope, $\Delta\nu$ is the bandwidth of channel, t_i is the total integration time; in the low frequency (~ 100 MHz) range the system temperature T_{sys} is dominated by the Galactic synchrotron background and scales as $\nu^{-2.5}$, or in terms of redshift (Chen & Miralda-Escudé 2006, Furlanetto et al. 2006b)

$$T_{sys} \simeq 2000 \left(\frac{1+z}{21} \right)^{2.5} \text{ K}. \quad (14)$$

For a conservative estimate we take the bandwidth of a channel $\Delta\nu = 4$ MHz, as a typical value for future telescopes. The effective area of the telescopes varies from $\sim 3 \times 10^4 \text{ m}^2$ for LOFAR (at 75 MHz) to 10^6 m^2 for SKA and LWA (for LUDAR it can reach up to $\sim 10^7 \text{ m}^2$). The optical depth in 21 cm increase from 10^{-3} at $z \simeq 10$ to 0.01 at $z \geq 15$ (Furlanetto 2006). Therefore, for the redshifts $z \geq 10$ we are interested in τ can be taken $> 10^{-3}$. The integration time is assumed to be of 10 weeks. Thus, the minimum background flux is 12 mJy at $z = 20 - 40$ for LOFAR, 0.4 mJy at $z = 20$ for SKA and LWA, and 2.3 mJy at $z = 40$ for LWA. In the case of UHECRs the difference of a smooth signal expected between the models with $\epsilon \geq 0.3 - 3$ is ≥ 5 mJy, and is even larger in the models with decaying dark matter. This supports the conclusion that observations on future telescopes can discriminate between the standard model and those affected by UHECRs and decaying particles.

5 CONCLUSIONS

In this paper we have considered the influence of UV photons from decaying dark matter particles and UHECRs on the ability of neutral hydrogen to emit and/or absorb in 21 cm at redshifts $z = 10 - 50$. We have found that

- the three sources of additional ionizing photons: long living and short living unstable dark matter particles and UHECRs produce fairly distinct dependences of the all-sky brightness temperature on redshift $T_b(z)$ – the first and the third give negative and positive second derivatives of the curves $T_b(z)$, while the second has $T_b(z)$ with an inflection point. Although the all-sky 21 cm emission is expected to be swamped by the overwhelming foreground signal, one

can hope that due to the lack of features in frequency space the latter can be removed. Moreover, the maps of the power spectrum of the brightness temperature on the wavenumber-redshift plane, reveal clear differences (seen in gradients of the temperature power spectrum over redshift) between various models of the particles.

- these features manifest in the frequency space of 21 cm line. From this point of view three wave-band observations at λ_1 , λ_2 and λ_3 and a “two-color” diagram for the relative (with respect to the foreground emission at a given wavelength) all-sky temperature differences $\Delta^2 T_{23} = \Delta T_b(\lambda_2) - \Delta T_b(\lambda_3)$ versus $\Delta^2 T_{12} = \Delta T_b(\lambda_1) - \Delta T_b(\lambda_2)$ can provide an additional tool for discrimination between the sources of ionizing photons in the end of dark ages.

In general, decaying dark matter particles can have strong effects on overall history of the universe: they may change its thermal evolution and cosmological nucleosynthesis (Scherrer 1984, Vayner et al 1985, Vayner & Shchekinov 1986), dynamics of large scale structure formation (Doroshkevich et al 1989, Bharadwaj & Sethi 1998, Cen 2001), reionization regime (Sciama 1982, Dodelson & Jubas 1994, Hansen & Haiman 2004, Chen & Kamionkowski 2004, Kasuya et al 2004, Kasuya & Kawasaki 2004, Pierpaoli 2004, Mapelli et al 2006), and even formation of the first stars though enhancement of H_2 molecule formation (Shchekinov & Vasiliev 2004, Vasiliev & Shchekinov 2006, Biermann & Kusenkov 2006, Ripamonti et al 2007, Furlanetto et al. 2006a). 21 cm emission from the epochs ending the dark ages can carry the imprints from decaying particles, and seems a promising tool for understanding their properties. Future radio telescopes (such as LOFAR, 21CMA, MWA, LWA and SKA) seem to have sufficient flux sensitivity for detection the signal in 21 cm influenced by decaying particles and UHECRs.

6 ACKNOWLEDGEMENTS

We thank the anonymous referee for valuable criticism. This work is supported by the Federal Agency of Education (project code RNP 2.1.1.3483) and by the RFBR (project code 06-02-16819-a).

REFERENCES

Barkana R., & Loeb A., 2005a, ApJ, 624, L65
 Barkana R., & Loeb A., 2005b, MNRAS, 368, L47
 Berezhinsky V.S., Kachelrieß M. & Vilenkin A., 1997, Phys. Rev. Lett., 79, 4302
 Biermann P.L., & Kusenkov A. 2006, Phys. Rev. Lett. 96i, 1301
 Bharadwaj S., Sethi S., 1998, ApJS, 114, 37
 Birkel, M. & Sarkar, S., 1998, Astropart. Phys., 9, 298
 Carilli C.L., 2006, NewAR, 50, 162
 Cen R., 2001, ApJL, 546, 77
 Cen R., 2003, ApJL, 591, L5
 Chen, X. & Kamionkowski, M., 2004, Phys. Rev. D, 70, 043502 (CK)
 Chen X. & Miralda-Escudé J., 2004, ApJ, 602, 1
 Chen X. & Miralda-Escudé J., 2006, submitted to ApJ, astro-ph/0605439
 Ciardi B., Ferrara A., White S.D.M., 2003, MNRAS, 344, L7
 Ciardi B. & Madau P., 2003, ApJ, 596, 1

Choudhury T.R. & Ferrara A., 2006, preprint (astro-ph/0603149) (to be published by RSP), edited by R. Fabbri
 de Bernardis P., Ade P.A.R., Bock J.J., Bond J.R., Borrill J., Boscaleri A., Coble K., Crill B.P. et al, 2000, Nature, 404, 955
 Di Matteo T., Perna R., Abel T., Rees M. J., 2002, ApJ, 564, 576
 Dodelson S., Jubas J.M., 1994, MNRAS, 266, 886
 Doroshkevich A.G., Khlopov M.Yu. & Klypin A.A., 1989, MNRAS, 239, 923
 Doroshkevich, A.G., & Naselsky, P.D., 2002, Phys. Rev. D, 12, 123517
 Doroshkevich, A.G., Naselsky, I.P., Naselsky, P.D., Novikov, I.D., 2003, ApJ, 586, 709
 Field G.B., 1958, Proc. IRE, 46, 240
 Furlanetto S. R., 2006, MNRAS, 370, 1867
 Furlanetto S. R., Oh S. P., Pierpaoli E., 2006a, Phys. Rev. D, 74, 103502
 Furlanetto S. R., Oh S. P., Briggs F. H., 2006b, Phys. Rept., 433, 181
 Gnedin N. Y. & Shaver P. A., 2004, ApJ, 608, 611
 Hanany S., Ade P., Balbi A., Bock J., Borrill J., Boscaleri A., de Bernardis P., Ferreira P.G. et al, 2000, ApJ, 545L, 5
 Hansen, S.H., & Haiman, Z., 2004, ApJ, 600, 26
 Hirata C. M., & Sigurdson K., 2007, MNRAS, 375, 1241
 Hogan C.J. & Rees M.J., 1979, MNRAS, 188, 791
 Kasuya S. & Kawasaki M., 2004, Phys. Rev. D, 70, 103519
 Kasuya S., Kawasaki M. & Sugiyama, N., 2004, Phys. Rev. D, 69b, 3512
 Kuhlen M., Madau P., Montgomery R., 2006, ApJ, 637L, 1
 Kuzmin, V.A., & Rubakov, V.A., 1998, Phys. Atom. Nucl., 61, 1028
 Liszt H., 2001, A&A, 371, 698
 Loeb A. & Zaldarriaga M., 2004, Phys. Rev. Lett. 92, 211301
 Madau P., Haardt F., Rees M.J., 1999, ApJ, 514, 648
 Madau P., Meislin A., Rees M.J., 1997, ApJ, 475, 492
 Mapelli M., Ferrara A., Pierpaoli E., 2006, MNRAS 369, 1719
 Miralda-Escudé J. & Rees M.J., 1994, MNRAS, 266, 343
 Oh S.P., 2001, ApJ, 553, 499
 Oh S. P., & Mack K. J., 2003, MNRAS, 346, 871
 Peebles P.J.E., Seager S., Hu W., 2000, ApJL, 539, L1
 Pierpaoli E., Phys. Rev. Lett., 2004, 92, 031301
 Ricotti M. & Ostriker J., 2004, MNRAS, 352, 547
 Ripamonti E., Mapelli M., Ferrara A., 2007, MNRAS, 375, 1399
 Scherrer R. J., 1984, MNRAS, 210, 359
 Sciama, D.W., 1982, MNRAS, 198, 1
 Scott D., Rees M.J., Sciama D., 1991, A&A, 250, 295
 Seager S., Sasselov D.D., Scott D., 1999, ApJ, 523L, 1
 Sethi S., 2005, MNRAS, 363, 818
 Shapiro P.R. & Giroux M.L., 1987, ApJL, 321, L107
 Shaver P. A., Windhorst R. A., Madau P., & de Bruyn A. G., 1999, A&A, 345, 380
 Shchekinov Yu. A. & Vasiliev E. O., 2004, A&A, 419, 19
 Shull J.M. & van Steenberg M.E. 1985, ApJ, 298, 268
 Spergel D.N., Verde L., Peiris H.V., Komatsu E., Nolte M.R., Bennett C.L., Halpern M., Hinshaw G., et al, 2003, ApJS, 148, 175
 Spergel D.N., Bean R., Doré O., Nolte M.R., Bennett C.L., Dunkley J., Hinshaw G., Jarosik N., et al, 2006, astro-ph/0603449
 Tegmark M., Silk J., Blanchard A., 1994, ApJ, 434, 395
 Tozzi P., Madau P., Meislin A., Rees M.J., 2000, ApJ, 528, 597
 Tumlinson J., Venkatesan A., Shull J.M., 2004, ApJ, 612, 602
 Vasiliev E. O. & Shchekinov Yu. A., 2006, Astr. Rept., 50, 778
 Vayner B.V. & Shchekinov Yu.A., 1986, SvA, 30, 480
 Vayner B.V., Shchekinov Yu.A. & Entel M.B., 1985, Ap, 23, 733
 Wouthuysen S. 1952, AJ, 57, 31
 Wyithe J.S.B. & Loeb A. 2003, ApJL, 588, L69
 Zaldarriaga M., Furlanetto S.R., Hernquist L., 2004, ApJ, 608, 622

